Real-time Measurement of Li-Ion Battery Cells Using Power Converter Pulse-Signal Injection and Fusion Methods

Irene Peláez, Pablo García, Geber Villa and Sara Saheed
Dept.of Electrical, Electronics, Systems & Computers Engineering
University of Oviedo, LEMUR Group
Gijón, 33204, Spain
Email: pelaezirene@uniovi.es,garciafpablo@uniovi.es,villageber@uniovi.es and saeedsarah@uniovi.es

***Abstract*—This paper proposes a method to estimate the impedance of Lithium-Ion cells by using an excitation signal. The injection signal is intended to be delivered to the battery module by the power converter used for the interface of the energy storage and using the current and voltage measurements provided by the module battery management system. The estimation method is conducted in two steps. During the system commissioning, the impedance is estimated by using a frequency-domain method known as vector fitting. Despite its high accuracy, it has an important computational burden that makes it difficult to use in real-time applications running on the embedded systems often used for battery and converter control. For that reason, during the regular operation, a recursive least squares algorithm is proposed, being the initial estimation given by the frequency-domain method employed during the commissioning process. The discussion includes not only the description and testing of the method but also the effects due to the reduced digital-domain resolution of the acquired data used for the estimation (terminal current and cell voltage), as well as the discretization method used for the digital implementation. The proposal is validated by simulation and by experimental results using the cell measurements provided by a BMS of a commercial module.**

I. Introduction

Lithium-Ion batteries have become a competitive storage technology in the market while their price keeps decreasing [1]. One of the critical parts of the battery that has a clear impact on its performance is the inner impedance. Power management, state of charge (SoC), state of health (SoH) are all affected by this impedance [1].

In the literature, different excitation inputs have been used for impedance estimation [2]. DC current pulse injection is the most common technique used for measuring the inner resistance and evaluate the degradation, and the only one accepted by standards for determining the power capability [3], [4]. It has to be remarked that the obtained impedance is also sensitive to the amplitude and pulse width [5], which in turn determines the frequency resolution [6]. The discussion presented in this paper evaluates in detail how both properties impact the estimation accuracy.

Regarding the digitalization process for the electrical variables used in the estimation, the sampling frequency, the resolution of the analog to digital converters, and the discretization method can degrade the estimation [7]. Details about the employed acquisition system and its effect on the estimation accuracy are given later in this paper. About the discretization, zero-order-hold (ZoH) transformation gives the exact discrete approximation, however, it requires a high computational burden when dealing with adaptive filters [8]. For that reason, backward Euler and Bilinear approximation, which ensure a stable transformation, will be compared in this paper.

Considering the equivalent electrical circuit for a Li-ion battery [9], [10], the inner parameters depend on the battery operation condition and aging condition [11]. Online estimation techniques based on adaptive filtering methods have been successfully implemented in the modeling of unknown systems [12]. Within the variety of adaptive filter alternatives, Kalman filter-based approaches are widely used for state estimation. However, they require a high computational burden when the system order is increased due to the matrix inverse calculation. On top of that, simultaneous estimation of system state and parameters is an endeavor task [7].

Recursive Least Squares (RLS) algorithm is an adaptive filter extensively used for parameter identification [7], [13], [14]. Different model identification methods which rely in RLS filter are compared in Table I. VFF-RLS [14] uses a variable forgetting factor and has a robust performance. However, the random parameter initialization increases the convergence time. In [13], it is included an inner-loop that performs an estimation multiple times between updates. It uses previously identified data and it is reported to improve the accuracy and to achieve a fast convergence. DWRLS method [7] was introduced to improve the estimation process and the noise robustness by separating the contribution to the dynamic response by the different parameters. The initialization process is done using approximated parameter values and, as reported

The present work has been partially supported by the predoctoral grant programs Severo Ochoa and FPU for the formation in research and university teaching of Principado de Asturias PCTI-FICYT under the grant ID PA-17-PF-BP16133 and Spain MECD under the grant ID FPU16/06829. This work also was supported in part by the Research, Technological Development and Innovation Program Oriented to the Society Challenges of the Spanish Ministry of Economy and Competitiveness under grant MCIU-18-RTC-2017-6338-3 and MCI-20-PID2019-111051RB-I00, by the European Union through ERFD Structural Funds (FEDER) and H2020 Research and Innovation programme under Grant Agreement No 864459 (UE-19-TALENT-864459). The present work was also supported by Cegasa Energía.

by the authors, very accurate results are shown. However, it also requires offline training. All of the reviewed methods have been tested only under laboratory conditions, although in [7], the simulation includes noise magnitude close to the expected levels when employing measurement systems typically used in commercial battery management systems (BMS). Still, it does not account for the finite digital resolution in the acquisition system.

TABLE I
IDENTIFICATION METHODS BASED ON RLS FILTER.

Method	Unknown Parameters	Discrete method	Convergence time [s]	Initialization	Battery type	Test bench
VFF-RLS [14]	4	Bilinear	> 30	Random	NMC	Lab
Inner-loop [13]	5	Backward	< 5	Matlab	LFP	Lab
DWRLS [7]	5	ZoH	> 5	Approx.	NCA	Lab
Proposed	5	Bilinear	< 5	VF	LFP	Commercial

As reported in the literature, the initialization process for the parameters is of critical importance to achieve correct results, otherwise the estimation might lead to high fluctuations or unreasonable values [13]. The long-established offline parametrization, based on least square (LS), is sensitive to noise and has been reported not to be the best of its class solution [7]. On the other hand, rational approximations provide a better estimation for higher-order systems, where particularly vector fitting (VF) [15] leads to more stable and robust results with respect to similar rational approximations schemes [16].

This paper presents a novel fusion method that initializes the parameter values of the RLS filter during the commissioning process with a frequency-domain method VF [15]. The initialization allows for a speed up in the convergence time and increased robustness [13]. To decouple the higher-order dynamics and make the method more robust under noise measurements, a sequential approach is proposed during the real-time estimation. The two networks are independently estimated by using an adaptive pulsed-injection signal, in which the period is changed according to the time constant being estimated.

The research of this paper contributes to the implementation of the identification method in a commercial system rather than relying on high accuracy laboratory equipment. Considering the target energy storage usage to be stationary applications, a two-level control system architecture is considered. At the battery module-level, a BMS for the cell-level monitoring, responsible of measuring the cell voltages and temperatures is considered. For higher-level variables and control needs, including system-level SoC, SoH and equalization, the BMS measured values are sent to a control system (EMS), either at string or system-level at much reduced sampling rates. The EMS typically incorporates the total current and voltage measurements.

Under that scenario, the most remarkable contributions of the present work include: 1) the effects of discretization approximations in the estimation when considering measurements limitations and 2) the validation of the proposed parameter identification approach using a commercial module and its BMS/EMS measurements instead of more common works based on a laboratory test-bench. The additional difficulties include a larger measurement noise as well as reduced resolution (1 mV for the voltage and 0.3 A for the current measurements) and the real-time implementation feasibility due to the use of CAN bus communication protocol between the BMS and the EMS, where the proposed method is implemented.

The research in this paper was first presented in a preliminary work in [17]. The results presented there have been extended in the following directions: 1) the implementation of the real-time discrete equations for the estimation process; 2) an enhanced method for increasing the system sensitivity to the independent parameter variation; 3) validation of the proposed approach using a commercial module and the internal BMS measurements at cell level.

The present paper is organized as follows: In Section II the continuous-domain model proposed for the battery impedance and the discretization process are introduced. In Section III, the parameter estimation methods, and the effects of the input signal parameters, pulse width, and frequency, are analyzed. In Section IV, the simulation and experimental results are exposed. To summarize, the conclusions obtained are gathered at the end of the paper.

II. SYSTEM MODELING

The chemical reactions that take place in Lithium-Ion batteries can be modeled by the equivalent circuit shown in Fig. 1 [9], [10]. R_s represents the cabling connections and the inner resistance of the battery and it grows with aging [18]. The capacitive effects in the surface of the electrode are captured by the first RC branch, while the second RC branch represents the diffusion processes of the electrolyte [10]. The fast branch has a time constant (τ_1) of a few seconds, whereas the slow one (τ_2) is in the range of hundreds of seconds [9]. These two very different dynamics are explored in this paper for easing the estimation process.

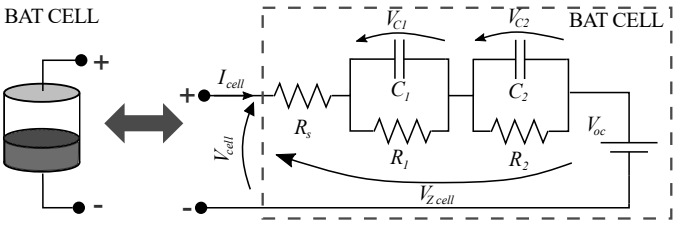

Fig. 1. Battery cell equivalent circuit.

The continuous domain transfer function for the impedance follows the relation in (1) with the coefficients of (2). To conduct the estimation in a digital system, a discrete approximation for the continuous-domain representation is needed. As before mentioned, the ZoH discretization that provides the exact value has a high computational burden. Thus, Backward Euler and Bilinear transformation (Table II) are proposed for the implementation. For the proposed equivalent circuit, the transfer function in the continuous-domain, the corresponding coefficients, and the discrete approximation are shown in (1)-(3) [19]. This approach is only valid for linear time-invariant

TABLE II
DISCRETE EQUIVALENTS BY NUMERICAL INTEGRATION.

	Backward Euler [13]	Bilinear [14], [19]
	$s \approx \frac{z-1}{zTs}$	$s \approx \frac{2}{Ts}\frac{(z-1)}{(z+1)}$
b_{0z}	$(R_1T_s^2 + R_2T_s^2 + R_sT_s^2 + C_1R_1R_2T_s + C_2R_1R_2T_s + C_1R_1R_sT_s + C_2R_2R_sT_s + C_1C_2R_1R_2R_s)/den_{bk}^*$	$(R_1T_s^2 + R_2T_s^2 + R_sT_s^2 + 2C_1R_1R_2T_s + 2C_2R_1R_2T_s + 2C_1R_1R_sT_s + 2C_2R_2R_sT_s + 4C_1C_2R_1R_2R_s)\ /den_{bi}^{**}$
b_{1z}	blue $-((C_1R_1R_2 + C_2R_1R_2 + C_1R_1R_s + C_2R_2R_s)T_s + 2C_1C_2R_1R_2R_s)/den_{bk}^*$	$(2R_1T_s^2 + 2*R_2T_s^2 + 2R_sT_s^2 - 8C_1C_2R_1R_2R_s)\ /den_{bi}^{**}$
b_{2z}	$(C_1C_2R_1R_2R_s)/den_{bk}^*$	$(R_1T_s^2 + R_2T_s^2 + R_sT_s^2 - 2C_1R_1R_2T_s - 2C_2R_1R_2T_s - 2_C1R_1R_sTs - 2C_2R_2R_sT_s + 4C_1C_2R_1R_2R_s)\ /den_{bi}^{**}$
a_{1z}	$-(C_1R_1(T_s + C_2R_2) + C_2R_2(T_s + C_1R_1))/den_{bk}^*$	$(2R_1T_s^2 + 2R_2T_s^2 + 2R_sT_s^2 - 8C_1C_2R_1R_2R_s)\ /den_{bi}^{**}$
a_{2z}	$C_1C_2R_1R_2/den_{bk}^*$	$(R_1T_s^2 + R_2T_s^2 + R_sT_s^2 - 2C_1R_1R_2T_s - 2C_2R_1R_2T_s - 2C_1R_1R_sT_s - 2C_2R_2R_sT_s + 4C_1C_2R_1R_2R_s)\ /den_{bi}^{**}$
$b_{0z\,rc}$	$(R_1T_s)/(R_1T_s + T_s)$	$(R_1T_s)/(T_s + 2C_1R_1)$
$b_{1z\,rc}$	0	$(R_1T_s)/(T_s + 2C_1R_1)$
$a_{1z\,rc}$	$(T_s - 2R_1C_1)/(2R_1C_1 + T_s)$	$(T_s - 2C_1R_1)/(T_s + 2C_1R_1)$
$b_{0z\,rcr_s}$	$(R_1T_s + R_sT_s + C_1R_1R_s)/(T_s + C_1R_1)$	$(R_1T_s + R_sT_s + 2C_1R_1R_s)/(T_s + 2C_1R_1)$
$b_{1z\,rcr_s}$	$-(C_1R_1R_s)/(T_s + C_1R_1)$	$(R_1T_s + R_sT_s - 2C_1R_1R_s)/(T_s + 2C_1R_1)$
$a_{1z\,rcr_s}$	$-(C_1R_1)/(T_s + C_1R_1)$	$(T_s - 2C_1R_1)/(T_s + 2C_1R_1)$

$^*den_{bk} = (T_s + C_1R_1)(T_s + C_2R_2)$
$^{**}den_{bi} = (T_s + 2C_1R_1)(T_s + 2C_2R_2)$

systems [20]. Both transformations are compared in the next section. The corresponding coefficients of (4) [19] for each of the approximations are gathered in Table II. The coefficients of the difference equation for one RC branch (5) [19], and one branch in series with the series resistor (6) [19] are also included in Table II for later discussion.

$$Z(s) = \frac{b_{0s}s^2 + b_{1s}s + b_{2s}}{a_{0s}s^2 + a_{1s}s + a_{2s}} \tag{1}$$

$$\begin{aligned} b_{0s} &= R_sR_1C_1R_2C_2; \\ b_{1s} &= R_s(R_1C_1 + R_2C_2) + R_2R_1(C_1 + C_2); \\ b_{2s} &= R_s + R_1 + R_2; \\ a_{0s} &= R_1C_1R_2C_2; \\ a_{1s} &= R_1C_1 + R_2C_2; \\ a_{2s} &= 1; \end{aligned} \tag{2}$$

$$Z_{cell}(z) = q\frac{V_{Z_{cell}}(z)}{I(z)} = \frac{b_{0z}z^2 + b_{1z}z + b_{2z}}{z^2 + a_{1z}z + a_{2z}} \tag{3}$$

$$\begin{aligned} V_{Z_{cell},k} = b_{0z}I_{cell,k} + b_{1z}I_{cell,k-1} + b_{2z}I_{cell,k-2} \\ - (a_{1z}V_{Z_{cell},k-1} + a_{2z}V_{Z_{cell},k-2}) \end{aligned} \tag{4}$$

$$V_{C,k} = b_{0z\,rc}I_{cell,k} + b_{1z\,rc}I_{cell,k-1} - a_{1z\,rc}V_{Z_{cell},k-1} \tag{5}$$

$$V_{CR_s,k} = b_{0z\,rcr_s}I_{cell,k} + b_{1z\,rcr_s}I_{cell,k-1} - a_{1z\,rcr_s}V_{Z_{cell},k-1} \tag{6}$$

TABLE III
LITHIUM-ION MODULE PARAMETERS

R_s [mΩ]	R_1 [mΩ]	C_1 [F]	τ_1[s]	R_2 [mΩ]	C_2 [F]	τ_2[s]
24	0.6	5630	3.3	8.2	54277	445

III. PARAMETER ESTIMATION

A. Power Converter Implementation

This work is intended for batteries connected to a dc/dc power converter capable of controlling the battery current using current regulation. This current-control capability allows for delivering current pulses to stimulate the battery impedance for identification purposes, as shown in Fig. 2. The battery impedance has to be sensitive to the excitation signal, thus the parameters can be identified in frequency and time domain. The dynamics of the system ought to be estimated are far from the current bandwidth of a dc/dc converter, typically in the range of hundreds of Hertz's, so these bandwidth effects are omitted. As a first approach, the parameters obtained for a Lithium-Ion battery module of 100 Ah following the same equivalent circuit model [21] collected in Table III are used to evaluate the estimation performance by simulation.

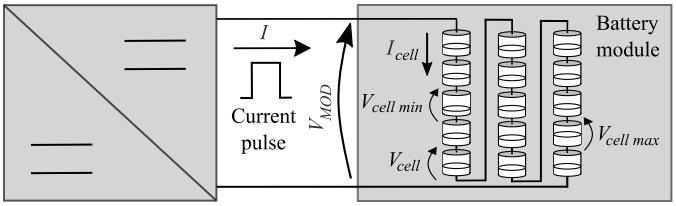

Fig. 2. Scheme for the connection of the converter to the battery terminals.

B. Estimation

1) Vector fitting: VF method seeks to conduct the estimation in the frequency domain by using the frequency spectrum of the impedance response [22]–[24], which is obtained from the cell battery voltage (V_{cell}) and current (I_{cell}). This current coincides with the total one (I) due to the series connection. From the impedance frequency spectrum, the method finds the coefficients of the transfer function in (7), where s is the Laplace variable and a_n the system poles, which closest matches the impedance calculation from the measurements. According to the proposed battery impedance model shown in (1), this impedance consists of two poles and the E component in (7) is 0, resulting in the transfer function in (8). The coefficients in (8) are related to the battery equivalent circuit parameters as stated in (9)-(13).

$$f(s) \simeq \sum_{n=1}^{N} \frac{c_n}{s - a_n} + D + sE \tag{7}$$

$$\begin{aligned} f(s) &= C \cdot (sI - A)^{-1} \cdot B + D + sE \\ &= \frac{b_2s^2 + b_1s + b_0}{(s - a_1)(s - a_2)} + D \end{aligned} \tag{8}$$

$$R_s = D \quad (9) \quad R_1 = b_0 - R_2 \quad (10) \quad C_1 = -\frac{1}{R_1 a_1} \quad (11)$$

$$R_2 = \frac{b_1 + \frac{1}{a_2} b_0}{\frac{-1}{a_1} + \frac{1}{a_2}} \quad (12) \qquad C_2 = -\frac{1}{R_2 a_2} \quad (13)$$

The digital implementation of the VF aims to get the impedance at the cell level, following the scheme in Fig. 3 and Alg. 1. The same scheme could be used at a module level if the global measurements are used, but the contribution of electrical connections will be more relevant in the final impedance. First (Step 1), the cell voltage (V_{cell}) and cell current (I_{cell}) measurements coming from the BMS/EMS are allocated in two memory buffers. The battery is considered to be at rest state at the beginning of the test, which corresponds to 2 h of no operation. The DC voltage component, V_{oc}, is compensated before the excitation signal starts, in order to isolate the impedance response of a cell, $V_{Z_{cell}}$, to the applied pulse.

Following step 2 in Fig. 3, the frequency-domain impedance is calculated from the compensated cell voltage ($V_{Z_{cell}}$) and current (I_{cell}). Step 2 of Alg. 1 (line 2) describes how the impedance module (Z_{mod}) and phase (Z_{ph}) is obtained at the frequency vector (Z_f) from the discrete Fourier transform (DFT).

Step 3 of Alg. 1 (line 10) and Fig. 3 gather the VF implementation. As mentioned before, the VF algorithm is launched using the implementation published in [22]. The algorithm requires the system order (n_o) and the number of iterations (N_{iter}). It is also defined the option of number of zeros, where, following the transfer function shown in (8), the matching with the proposed model corresponds to $D \neq 0$ and $E = 0$. The resulting state space system is obtained in the SER variable after the call to the VF function. The coefficients are matched to the given transfer function (9)-(13) to obtain the needed parameters.

To obtain a crisp resolution in the frequency domain, the different natural frequencies for the system dynamics have to be captured. According to the definition of frequency resolution in discrete systems, $f_{res} = \frac{1}{NT_s}$, where N is the number of samples and T_s the sample time, this resolution should be low enough to identify the large time constants of the two RC branches. The following section will present a discussion for the f_{res} constrains.

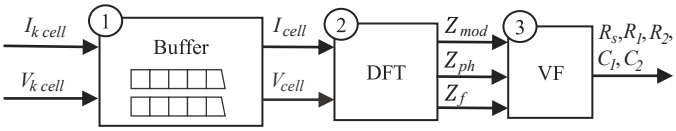

Fig. 3. Vector fitting implementation.

2) Recursive Least squares: The RLS algorithm is an adaptive filter that combines the least square estimation method plus the matrix inversion lemma [25]. As depicted in Fig. 4, this algorithm seeks to minimize a cost function (14) by recursively finding the coefficients w (15) of the n_0 order system from the measurements (16) using a forgetting factor λ and a weighted covariance matrix P. A white noise estimation ($\hat{e}_{k-1}$) is also considered to improve the results [26]

Algorithm 1: VF IMPLEMENTATION.

Input: I_{cell}, V_{cell}, T_s
Output: $\hat{R}_{s,0}$,$\hat{R}_{1,0}$,$\hat{R}_{2,0}$,$\hat{C}_{1,0}$,$\hat{C}_{2,0}$
1 $V_{Z\,cell} = V_{cell} - V_{oc}$;
// Step 2: DFT of Z_{cell}
2 V_{DFT}=DFT($V_{Z\,cell}$);
3 I_{DFT}=DFT(I_{cell});
4 N=length(V_{DFT}); f_{res}=1/($N \cdot T_s$); f_N=1/2/T_s;
5 Z_{ph}=angle(V_{DFT}) −angle(I_{DFT});// rad
6 $V_{DFT\,0}$=$V_{DFT\,0}$/2; $I_{DFT\,0}$=$I_{DFT\,0}$/2;
V_{mod}=abs(V_{DFT})/(N/2);I_{mod}=abs(I_{DFT})/(N/2);
7 Z_{mod}=V_{mod}./I_{mod};
8 Z_{mod}=$Z_{mod}(1 : f_N - f_{res})$; Z_{ph}=$Z_{ph}(1 : f_N - f_{res})$;
9 Z_f=$0 : f_{res} : f_N - f_{res}$;
// Step 3: Init VF
10 Z=Z_{mod}. $\cdot\, e^{jZ_{ph}}$;
11 $n_o = 2$; // number of poles
12 N_{iter}=5; // number of iterations
13 opts.stable=1; // Enforce stable poles
opts.asymp=2; // Fitting: $D \neq 0, E = 0$
14 N_s=length(Z);
15 Z_w=$Z_f \cdot 2\pi$;
16 $weigth$=ONES(N_s,1);
17 s=$j. \cdot Z_w$;
18 $poles$ =linespace($Z_{w,1}, Z_{w,end}, n_o$);
19 **for** N=1:N_{iter} **do**
20 [$SER, poles, err, datafit$]=
vecfit3(Z,s,$poles$,$weight$,$opts$)
21 **end**
22 [A,B,C,D]=[SER.A,SER.B,SER.C,SER.D];
23 ϕ=1/(s*linespace(length(A))-A);
24 f(s)=C·ϕ· B +D; // Eq.(8)
25 [$\hat{R}_{1,0}$,$\hat{R}_{2,0}$,$\hat{C}_{1,0}$,$\hat{C}_{2,0}$]=f(b_0,b_1,a_1,a_2)// Eqs.(9)–(13)

and its coefficient c_1 is initialized to 0. The RLS function implementation is collected in Alg. 2 and it allows to initialize the function with the previous n_0 measurement vectors (u_{k0}, y_{k0}), the coefficients (w_0) and the covariance matrix P_0. The updated coefficients w_k and estimated output $\hat{y}_k$ are updated every sampling time, from the current input (u_k) and output (y_k) measurements.

The impedance is considered time-invariant during each testing period. For the problem being, this only assumes that the impedance variation takes longer than the required estimation time. Otherwise, it is required to use the extended version of the filter [27]. As in the frequency case, the battery is considered to be at rest state at the beginning of the test and the initial DC voltage component (V_{oc}) is subtracted, so the remaining voltage corresponds to the voltage drop in the estimated impedance ($V_{Z_{cell}}$).

$$e = y_{k1} - x'_{RLS} \cdot w_{RLS} \quad (14)$$

$$w_{RLS} = [b_{0z}\, b_{1z}\, a_{1z} c_1] \quad (15)$$

$$x_{RLS} = \left[u_{k1},\, ...u_{k1-n_o},\, -y_{k1-1}, ... - y_{k1-1-(n_o-1)},\, \hat{e}_{k-1}\right] \quad (16)$$

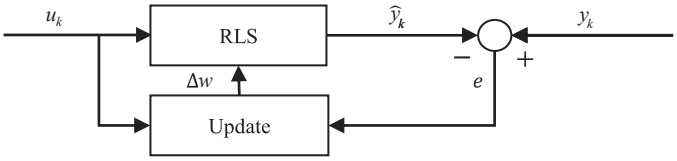

Fig. 4. Adaptive RLS algorithm.

The implementation of the proposed online estimation method is summarized in Fig. 5. The estimation avoids the direct use of (4) as the cost function to minimize the measurement noise over the estimation results. Instead, since the overall impedance has two-time constants at very different time orders, the system is split into two first-order systems ($n_o = 1$). This provides better access to the states (capacity voltages), which are easily decoupled from R_s. The impedance parameters obtained from the VF method are used to initialize the estimation. Firstly, the first (fastest) branch is estimated and after 5 times τ_1 (t_{ch}) [9], the estimation process switch to the second branch. R_s is estimated in both stages. During the estimation of the first branch parameters, the ones from the second branch are held constant at the last known (initially determined by the VF method) values and its voltage drop is subtracted to the measured voltage $V_{Z_{cell}}$. This difference is used as the voltage measurement in the RLS filter, so R_s and the first branch parameters are estimated using (6) as the cost function and following the relation in Table IV.

When the first branch estimation is concluded at t_{ch}, the $\hat{R}_{s\,m}$, $\hat{R}_{1\,m}$, $\hat{C}_{1\,m}$ mean values for the last τ_1 period are obtained. From there, the coefficients from Table II are used to compute the first branch voltage (5), initialize the coefficient w from the second branch voltage, and its initial voltage. After t_{ch}, the second branch parameters plus R_s follows the estimation steps of the first branch estimation. Each sampling time the estimated parameters are updated.

Algorithm 2: RLS FUNCTION.

$[\hat{y}_k, w_{out}]$=RLS$(\lambda, P_0, w_0, n_o, u_{k1}, y_{k1}, u_{k0}, y_{k0})$
$persistent\langle w_{1k}\, P_{1k}\, u_k\, y_k\, n_k\rangle$;
if $isempty(w_{k\,1})$ **then**
  $w_{1k} = w_0$; $P_{1k} = P0$; $u_k = zeros(1, n_o + 1)$;
  $y_k = zeros(1, n_o + 1)$; $n_k = zeros(1, n_o + 1)$;
  $u_k(2 : end) = u_{k0}$; $y_k(2 : end) = y_{k0}$;
$u_k(1) = u_{k1}$; $y_k(1) = y_{k1}$;
$x_k = [u_k, -y_k(2 : end))]$;
$e_k = y_k(1) - w_{1k}x_k$;// Cost function
$g_k = P_{1k}x_k[\lambda + x_k^T P_{1k}x_k]$;// gain update
$P_k = \lambda^{-1}P_{1k} - g_k x_k^T \lambda^{-1}P_{1k}$;// cov. update
$w_k = w_{1k} + e_k g_k$;// Coeff. est.
$\hat{e}_k = y_k(1) - w_k x_k$;// Est. error
$w_{1k} = w_k$;$P_{1k} = P_k$;
$u_k(2 : end) = u_k(1 : end - 1)$; $y_k(2 : end) = y_k(1 : end - 1)$; $n_k(2 : end) = n_k(1 : end - 1)$;
$\hat{y}_k = w_k x_k$; $w_{out} = w_k[1 : 3]$;
return w_{out}, $\hat{y}_k$;

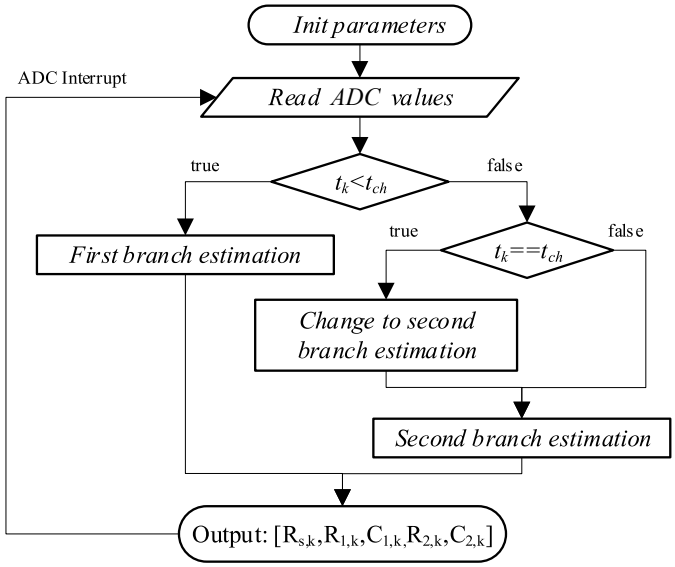

Init parameters

$[\hat{R}_{s,0},\hat{R}_{1,0},\hat{C}_{1,0},\hat{R}_{2,0},\hat{C}_{2,0}]$=VF($V_{test\,VF}$, $I_{test\,VF}$,$T_{s\,VF}$);
$\tau_1=\hat{R}_{1,0}\hat{C}_{1,0}$; $t_{ch}=5\tau_1$;$n_o=1$;
λ=0.991; $P_0=10^6$eye($2n_o$+3); c_1=0;
$[b_{0z\,RC1Rs}, b_{1z\,RC1Rs}, a_{1z\,RC1Rs}]$=f($\hat{R}_{s,0}$,$\hat{R}_{1,0}$,$\hat{C}_{1,0}$); *(Table II)*
$[b_{0z\,RC2}, b_{1z\,RC2}, a_{1z\,RC2}]$=f($\hat{R}_{2,0}$,$\hat{C}_{2,0}$); *(Table II)*
w_0=[$b_{0z\,RC1Rs}$,$b_{1z\,RC1Rs}$,$a_{1z\,RC1Rs}$,c_1];
u_{0k}=0; y_{0k}=0; t_k=0; $V_{cell,0}=V_{cell}$;

Read ADC values

$I_{cell,k}$, $V_{cell,k}$; *(ADC values)*
$V_{Zcell,k}=V_{cell,k}-V_{cell,0}$; $t_k=t_{k-1}+T_s$;

First branch estimation

$V_{C2}=I_{cell,k}b_{0z\,RC2}+I_{cell,k-1}b_{1z\,RC2}-V_{Zcell,k-1}a_{1z\,RC2}$;
$V_{C1Rs}=V_{Zcell,k}-V_{C2}$;
$[V_{C1R}, w_k]$=RLS(λ,P_0,w_0,n_0,$I_{cell,k}$,V_{C1Rs},u_{k0},y_{k0}); *(Alg. 2)*
$b_{0z}=w_{k,1}$; $b_{1z}=w_{k,2}$; $a_{1z}=w_{k,3}$;
$[\hat{R}_{s,k},\hat{R}_{1,k},\hat{C}_{1,k}]$=f($b_{0z}$,$b_{1z}$,$a_{1z}$); *(Table IV)*
$\hat{R}_{2,k}=\hat{R}_{2,0}$;$\hat{C}_{2,k}=\hat{C}_{2,0}$;

Change to second branch estimation

Clear RLS; ls=(t_k.τ_1):t_k;
$R_{s\,m}$=mean($\hat{R}_{s,1:ls}$); $R_{1\,m}$=mean($\hat{R}_{1,1:ls}$); $C_{1\,m}$=mean($\hat{C}_{1,1:ls}$);
$[b_{0z\,RC1}, b_{1z\,RC1}, a_{1z\,RC1}]$=f($R_{1\,m}$,$C_{1\,m}$); *(Table II)*
$V_{C1}=V_{C1R}-R_{s\,m}I_{cell,k-1}$;
$[b_{0z\,RC2Rs}, b_{1z\,RC2Rs}, a_{1z\,RC2Rs}]$=f($R_{2\,m}$,$C_{2\,m}$,$R_{s\,m}$); *(Table II)*
w_0=[$b_{0z\,RC2Rs}$,$b_{1z\,RC2Rs}$,$a_{1z\,RC2Rs}$,c_1]; $P_0=10^6$eye($2n_o$+3);
$y_{k0}=V_{C2}-R_{s\,m}I_{cell,k-1}$;
$u_{k0}=I_{cell,k-1}$;

Second branch estimation

$V_{C1}=I_{cell,k}b_{z0\,RC1}+I_{cell,k-1}b_{z1\,RC1}-V_{C1}a_{z1\,RC1}$;
$V_{C2Rs}=V_{Zcell,k}-V_{C1}$;
$[V_{C2R}, w_k]$=RLS(λ,P_0,w_0,n_0,$I_{cell,k}$,V_{C2Rs},u_{k0},y_{k0}); *(Alg. 2)*
$b_{0z}=w_{k,1}$; $b_{1z}=w_{k,2}$; $a_{1z}=w_{k,3}$;
$[\hat{R}_{s,k},\hat{R}_{2,k},\hat{C}_{2,k}]$=f($b_{z0}$,$b_{z1}$,$a_{z1}$); *(Table IV)*
$\hat{R}_{1,k}=R_{1\,m}$;$\hat{C}_{1,k}=C_{1\,m}$;

Fig. 5. RLS flowchart for the digital implementation.

TABLE IV
PARAMETER ESTIMATION FROM DIFFERENCE EQUATION COEFFICIENTS.

	Backward Euler	Bilinear
R_s	$b_{1z\,rcr_s}/a_{1z\,rcr_s}$	$-\frac{b_{0z\,rcr_s}-b_{1z\,rcr_s}}{(a_{1z\,rcr_s}-1)}$
R_1	$-\frac{b_{1z\,rcr_s}-a_{1z\,rcr_s}b_{0z\,rcr_s}}{a_{1z\,rcr_s}(a_{1z\,rcr_s}+1)}$	$-\frac{2(b_{1z\,rcr_s}-a_{1z\,rcr_s}b_{0z\,rcr_s})}{a_{1z\,rcr_s}^2-1}$
C_1	$\frac{T_s a_{1z\,rcr_s}^2}{b_{1z\,rcr_s}-a_{1z\,rcr_s}b_{0z\,rcr_s}}$	$\frac{(T_s(a_{1z\,rcr_s}-1)^2}{4b_{1z\,rcr_s}-4a_{1z\,rcr_s}b_{0z\,rcr_s}}$

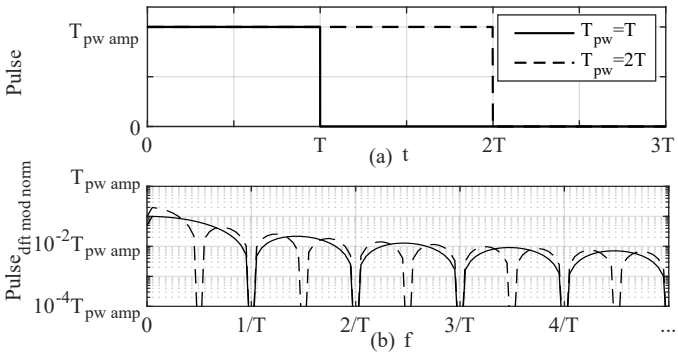

Fig. 6. Pulse relation with T_{pw} in a) time and b) frequency domain for two different T_{pw}.

C. Excitation signal selection criteria

1) Frequency domain: As explained before, the VF method runs in the frequency domain. In the literature, three excitation signals are commonly used: chirp, train of pulses or a single pulse [4]. The chirp signal has a constant magnitude over the frequency range it covers. The train of pulses will only cover the odd harmonics starting from the main frequency of the signal. This paper is focused on the low-frequency range, thus, the pulse response will be enough for obtaining the response at that range. This is also consistent with the online implementation and the delivery of the injection signal from the power converter, which makes the pulse-based implementation much simpler. This type of signal is used by standards to evaluate the cell inner resistance [3], where here it is also pretended to be used to further obtain the low-frequency dynamics. As mentioned before, to examine only the impedance, the initial voltage V_{oc} is subtracted from the overall V_{cell}.

Fig. 6 shows the module of the normalized DFT response for two pulse signals with same amplitude ($T_{pw\,amp}$) and two different (double) widths (T_{pw}). The lobes are related to T_{pw} following the relationships gathered in (17), where their module vanishes to zero at $1/T_{pw}$ and its harmonics and each lobe amplitude ($Lb_{i\,amp}$) is doubled with T_{pw}. Since the impedance estimation requires to divide the voltage frequency domain values by the corresponding current, frequencies at zero-crossing points have to be removed from the estimation. It is determined that values below 10% of the maximum current main amplitude will not be considered to tackle this issue.

$$Lb_{width} = \frac{1}{T_{pw}}; \quad Lb_{i\,amp} = \frac{Lb_{i\,amp\,1T}}{T_{pw}}; \tag{17}$$

The VF method has been tested for the battery impedance in Table III at different f_{res} and T_{pw} and the parameter errors obtained are collected in Fig. 7. The results are represented normalized by the respective RC branches time constants at the x-axis. The denormalized f_{res} tested correspond to different t_{end} of 6 to 50 minutes, which is equivalent to a f_{res} from 2.8 to 0.3 mHz. The selected pulse magnitude corresponds to a current rate (C_r) of 0.3C.

Fig. 7a-e presents the parameter estimation error when considering no measurement error and infinite resolution in the acquired signals. A lower f_{res} leads to a better estimation in the RC branches, where the slow branch becomes the most sensitive to this factor and increasing the relation $f_{res}\tau_2$ above 0.3 results in an error above 5%. In Fig. 7f-j, a finite resolution of 1 mV and 0.3 A is assumed in the measurements. This corresponds to typical resolutions in state-of-the-art BMS. The error given at low T_{pw} derives from the resolution of the voltage measurement mainly and it is combined with the error due to f_{res} mentioned before. On the other hand, R_s is perfectly estimated in any case and it is neither affected by T_{pw} and f_{res}.

Further considerations for establishing the test conditions in both variables are: 1) with regard to T_{pw}, it is desired to have the shortest possible duration, so the variation of SoC is minimized. 2) a higher f_{res} value will reduce the required test time. Based on the results, as a trade-off between the effect of both parameters, $T_{pw} = 15$ s and $f_{res} = 0.7$ mHz. This selection gives an overall estimation error below 5%.

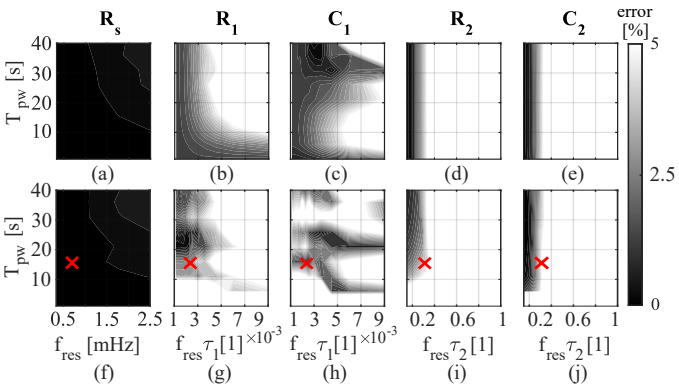

Fig. 7. Estimation error in terms of pulse width and normalized frequency resolution ($f_{res}\tau$) and pulse width (T_{pw}/τ) in the implementation for the VF method. Error of the estimation with infinite resolution: a)R_s, b) R_1, c) C_1, d) R_2, e) C_2. Error of the estimation when with a limited resolution of 1 mV and 0.3 A: f)R_s, g) R_1, h) C_1, i) R_2, j) C_2.

2) Time domain: For the RLS implementation, the shape of the input signal current has to be selected so the output voltage is sensible to the parameters sought to be estimated. For the signal excitation, a train of pulses is selected for this case since it allows a simple real-time digital-domain implementation and it has a good sensitivity at the output voltage for the parameter variation. Different simulations are performed following the pulse train scheme in Fig. 8a-b, with different test lengths (t_{end}) and T_{pw}. For branches with time constants that differ more than one decade, they do not interfere with each other, as can be seen in Fig. 8c-d, where the effects in the phase of both time constants are decoupled.

The equivalent circuit components are solved using Backward Euler and Bilinear transformations following the relation

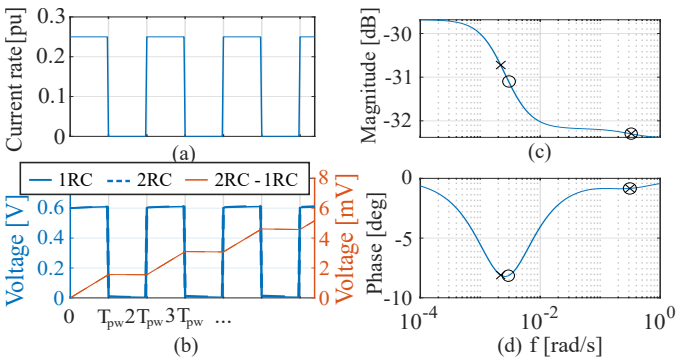

Fig. 8. Pulse train used for the RLS method. Pulses are current-controlled. a) Current rate (C_r) of the train pulse. b) Response of the impedance considering 2 branches (continuous line), 1 RC branch (dashed line), and their difference (red). Bode diagram of the system in Table III: c) Magnitude and d) Phase.

in Table IV. In this initial case, the noise is not accounted for to better understand the effect of the selected signal and the impact of the discrete transformation approach. The series resistance is perfectly estimated in both cases and it is not affected by the discretization, t_{end} and T_{pw}. Fig. 9a-h presents the resulting relative error of the dynamic branches estimation at the end of the simulation. As expected, the Bilinear approximation gives the best results due to the minimization of the signal shift. Fig. 9i-l presents the parametrization error when the limited resolution is applied as in the VF method, and it is found that there is a minimum pulse width required for the dynamic branches so the measurements are sensitive to the parameters. In this case, the series resistance is also perfectly estimated and not included in the figure.

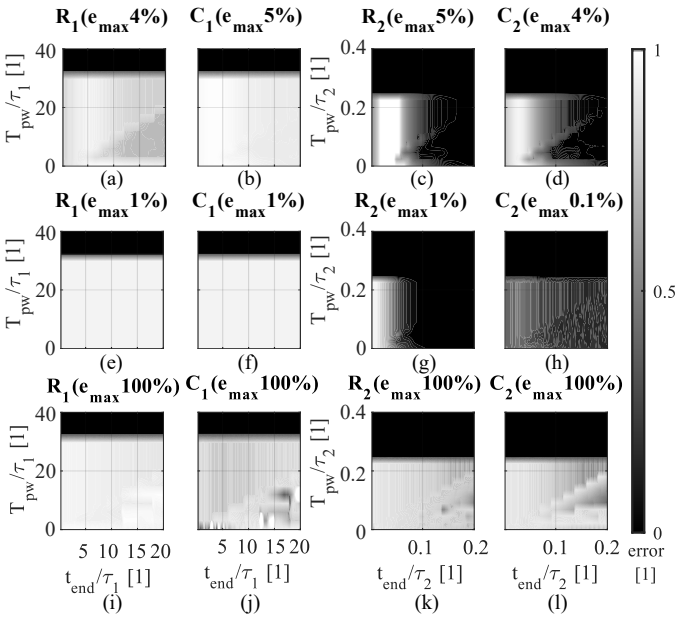

Fig. 9. Relative error of the estimation in terms of normalized pulse width (T_{pw}/τ) and test length (t_{end}/τ) for the RLS method. The error is normalized to each maximum absolute error indicated in each title (e/e_{max}) for the three cases: Backward Euler approach and infinite resolution: a) R_1, b) C_1, c) R_2, d) C_2; Bilinear approach and infinite resolution: e) R_1, f) C_1, g) R_2, h) C_2; Bilinear approach and a resolution of 1 mV and 0.3 A: i) R_1, j) C_1, k) R_2, l) C_2.

IV. Simulation and Experimental Results

A. Simulation results

The simulation results are presented herein. Both methods are evaluated considering the parameters of Table III.

1) VF results: The VF method is evaluated by analyzing the voltage and current response (Fig. 10a,c), after a current pulse. The current and voltage measurements have a resolution of 1 mV and 0.3 A respectively, which corresponds to the experimental setup presented in the next section. In Fig. 10b,d, the module of the current and voltage frequency response is shown. The impedance is calculated from their division, avoiding values below $0.1I_{max}$ for the estimation.

The resulting impedance used for VF is depicted in Fig. 10e, where it can be seen that at low-frequency values, the response used with the proposed f_{res} can capture the slow dynamics. The parameter values obtained are gathered in Table V. The overall error is below 5%, being slightly higher for the slow branch parameters, as it was expected from Fig. 7.

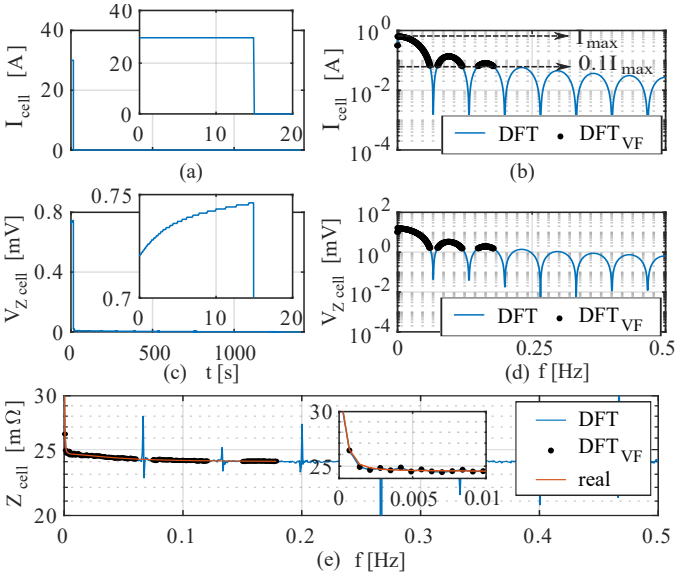

Fig. 10. Simulation results. a) Current pulse. b) DFT of the current pulse. c) Impedance voltage response. d) DFT of the impedance voltage response. Values below $0.1I_{max}$ are highlighted with black dots. e) Cell impedance module considering all the points (blue) and only using values above $0.1I_{max}$. The module with the real parameters is represented in red.

TABLE V
Simulation Results

	R_s[mΩ]	R_1[mΩ]	C_1[F]	R_2[mΩ]	C_2[F]
VF	24	0.61	5834	7.9	56942
error[%]	0.01	2.25	3.62	4.06	4.90
RLS	24	0.6	5769	8.3	60716
error[%]	0.01	0.8	2.48	1.70	11.86

2) RLS results: From the VF results, the initial parameters for the RLS implementation are obtained. For the RLS implementation, the sampling frequency is 10 Hz, the forgetting factor λ has been set to 0.991 and, the initial covariance diagonal terms P_{k-1} to 10^{10}. Two consecutive sequences of

current train pulses are used as the input signal. The first one has a period T_{pw} of τ_1 and it last up to t_{ch}. The period for the second sequence is $T_{pw} = 5\tau_1$, which allows for a decoupling of the first branch dynamics without requiring a long time for the estimation to converge. The dual-sequence current-injection pulses aim to energize closer harmonics to the branch being estimated.

Different cases are exposed in Fig. 11 to evaluate the influence of disturbance factors in the estimation. Case 1 depicts the results when the parameters are initialized with VF results and the resolution is infinite, so there is no error in the estimation (considering as no error the difference to the VF estimation). Case 2 shows the estimation results when the initial values to be estimated by the first RLS sequence are 20% lower. Finally, Case 3 includes the influence of finite resolution, which is set to 0.1 mV and 0.3 A for the cell-voltage and current respectively. This factor lets the first branch parameters reach convergence. However, it has a higher impact in the second branch, requiring a longer convergence time. Conclusions from this simple study are that the estimation is robust to the initial estimation errors but it can be noticeably affected by lower resolution in the measurement system, which is typically the case for commercial modules compared to the instrumentation used in laboratory conditions.

Fig. 12a-b presents the input current and voltage response. The measured voltage is compared to the simulated one with the final estimated parameters, which are obtained at the end of the test, as gathered in Table V. It can be seen in Fig. 12b that the estimated voltage tracks the real one when considering a linear-time invariant (LTI) system and using the final parameters of Table V, even when 1 mV and 0.3 A resolution is considered. The voltage error (Fig. 12c) has a negative trend and keeps below 1% when the pulse current is applied.

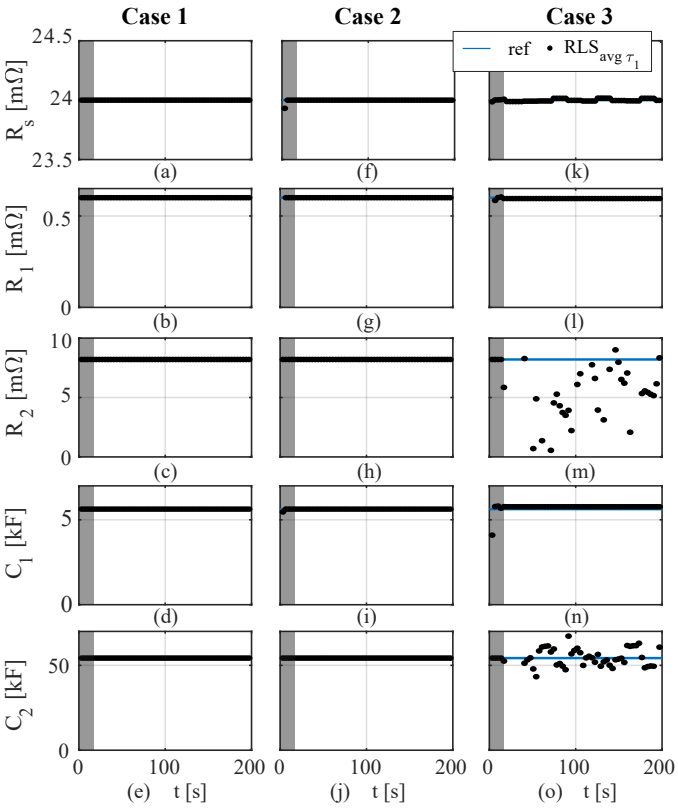

Fig. 11. Simulation results for the parameter estimation using the RLS method. Theoretical results are depicted in blue, estimated results averaged every τ_1 (3.3 s) are highlighted by black dots. The gray area corresponds to the estimation of the first RC branch and R_s, which it is ended at $5\tau_1$. Case 1 presents the estimation with the values given by VF for: a) R_s. b) R_1. c) R_2. d) C_1. e) C_2. Case 2 initialize the parameters to be estimated below $5\tau_1$ with a value 20% lower for: f) R_s. g) R_1. h) R_2. i) C_1. j) C_2. Case 3 includes the resolution effects of a commercial module for: k) R_s. l) R_1. m) R_2. n) C_1. o) C_2.

B. Experimental results

For the experimental setup, a commercial battery module of Cegasa Energía has been used (Fig. 13). The module consists of 15 LFP cells in series, where their properties are collected in table VI. To generate the injected current pulse, the module is connected to a bidirectional source DELTA SM 70-CP-450. The module is connected to a control unit (EMS) where the total current and bus voltage are measured. Each control unit can handle up to 8 modules connected in series. The module BMS communicates with the control unit via CAN-Open protocol and allows to get the main variables of the connected battery modules. The BMS samples the cell voltages at 27 kHz and they are filtered by two low-pass filters: the first one has a cutoff frequency of 7 kHz and the second one of 26 Hz. The control unit captures the current and voltage measurements instantaneously with a sampling time of 0.1 ms. Using the communications link, it only monitors in real-time the minimum and maximum cell voltage and temperature of each module, the ambient temperature, and the total current. The impedance estimation is carried out at cell level since it is not proportional the performance from cell to module level due to the heterogeneous operation of the cells [28]. The

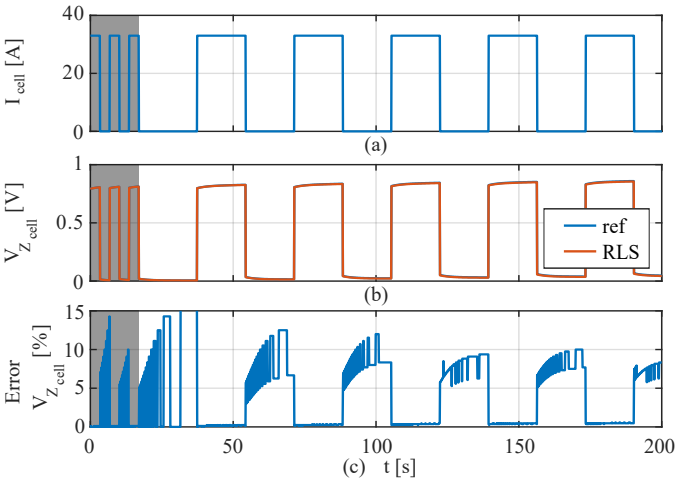

Fig. 12. Simulation results of the responses: a) Current pulses at 0.17 C_r. b) Impedance voltage using the estimated values are presented in red (RLS values of Table V) and the theoretical ones in blue. c) Resulting voltage error between the estimated and reference voltage. The gray area corresponds to the estimation of the first RC branch and R_s, which is ended at $5\tau_1$.

conducted experiments use the monitored cells at the lowest and highest voltage, which are the ones that reach faster the cutoff voltages, and are conducted with a 50% battery module SoC.

TABLE VI
CELL CHARACTERISTICS

Type	Q_{nom} $[Ah]$	V_n $[V]$	Z_{1000Hz} $[m\Omega]$	V_{min}-V_{max} $[V]$	C_r dis/ch
LFP	180	3.2	0.6	2.5 - 3.65	1.2/1

Fig. 13. Setup used for the experimental results. The battery module consists of 15 LPF cells in series.

1) VF estimation: The same input signal as in the simulation analysis is used, as shown in Fig. 14a. The response of a battery cell is gathered in Fig. 14c,e for cells having maximum and minimum voltage. It can be observed that the voltage resolution (1 mV) becomes noticeable. The pulse signal has a T_{pw} of 15 s and a f_{res} of 0.7 mHz, which corresponds to a test length of 1430 s. The DFT of the current and voltage signals are obtained as presented in Fig. 14b,d,f, and from their division, the DFT of the impedance is obtained (Fig. 15a-b). As the current lobes draw towards zero, there is a distortion induced in the module of the impedance, which corresponds to lobes amplitude below 10% of the maximum current lobe. Values under this range are discarded and only the values presented in black dots in Fig. 14b,d,f are used for the estimation. The resulting parameters obtained following the scheme of VF implementation (Alg. 1) are collected in Table VII.

Figs. 15c-d show the error between the experimental and the module of the resulting Bode with the estimated parameters. The approach of the 2RC model results in an error below 0.1% for the frequency range tested.

2) RLS estimation: The real-time estimation is presented herein. For the test, the sequence of current-pulse trains presented in Fig 16a is used. The covariance matrix and λ maintain the same simulation values. The parameters of the VF estimation are used to initialize the method.

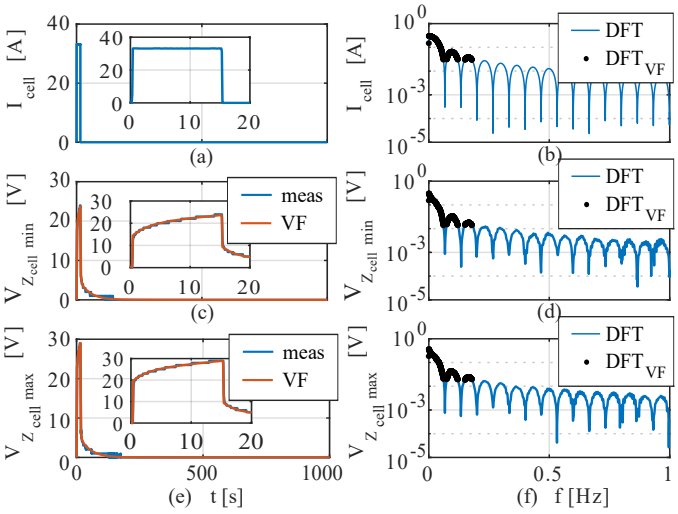

Fig. 14. Pulse injected for the VF estimation in time (left column) and frequency-domain (right column). The measure is represented in blue and the voltage response with the obtained estimated parameters in red. The black dots highlight the values above $0.1I_{max}$ used in the VF estimation, where the blue line represents the whole range. a) Current pulse in time-domain. b) DFT of the current pulse. c) Cell with minimum voltage. d) DFT of the cell with minimum voltage. e) Cell voltage with maximum voltage. f) DFT of the cell with maximum voltage.

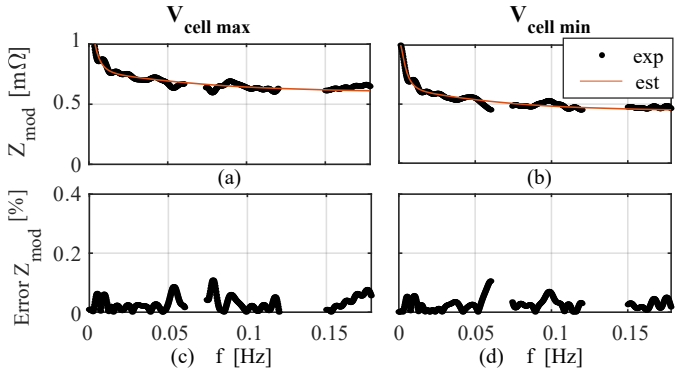

Fig. 15. Comparison between the module of the experimental results and system obtained with the estimated parameters (Table VII). a) Z_{mod} from the experimental data (black dots) and from the bode diagram using the estimated parameters (red) for: a) cell with maximum voltage, b) cell with minimum voltage. b) Error of the estimated system with respect to the experimental one for: c) cell with maximum voltage, d) cell with minimum voltage.

The estimated parameters in real-time are gathered in Fig. 17, where it can be seen that R_s (Fig. 17a-b) keeps similar to the initial guess of VF. However, the dynamics converge to different values from the initials and the second branch require around 80 s following the real-time estimation (Fig. 17c-j). Table VII gathers the average value of the parameters during the last τ_1 period of the test. It has to be noted that the initial VF guess does not represent the real parameter values, but only an approximation of those and that the typical use of the real-time impedance measurement is to track impedance changes due, mainly, to aging, temperature, and SoC factors. Considering that, the estimation is considered in a very good agreement.

In Fig. 16b,e, the resulting voltage with the estimated parameters of both methods (Table VII) and the measured

voltage for both cells are depicted. As has been mentioned, the initial guess of the parameters with the VF method does not meet the current situation of the battery. The reason for these discrepancies might come due to the non-linearities of the battery, which are not modeled here. However, for the test window considered, this linear approach of the 2 RC equivalent-circuit model achieves an error below 0.1%, as shown in Fig. 16c,f for the cell with the highest and lowest voltage respectively.

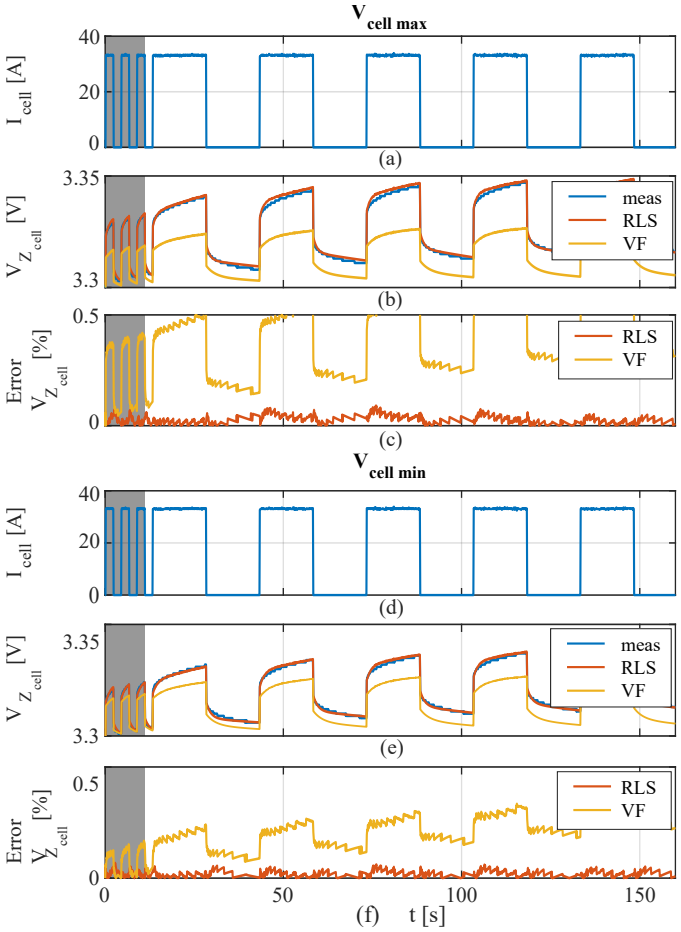

Fig. 16. Current and voltage evolution of the experimental results for the cells with the highest and lowest voltage. Highest voltage: a) Current-train pulse. b) Measured voltage (blue), voltage estimated with the final RLS parameters (red), voltage estimation using the initial commissioning parameters by the VF method (yellow). c) Voltage error by the linear approach using the real-time RLS (red) and the VF method (yellow). Lowest voltage: d) Current-train pulse. e) Measured voltage (blue), voltage estimated with the final RLS parameters (red), voltage estimation using the commissioning parameters obtained by the VF method (yellow). f) Voltage error by the linear approach using the real-time RLS (red) and VF method (yellow). The gray area corresponds to the estimation of the first RC branch and R_s, which is ended at $5\tau_1$.

TABLE VII
PARAMETERS ESTIMATED IN THE EXPERIMENTAL TEST

	case	R_s[mΩ]	R_1[mΩ]	C_1[F]	R_2[mΩ]	C_2[F]
VF	$V_{cell\,min}$	0.43	0.15	16439	0.45	94412
	$V_{cell\,max}$	0.59	0.14	15895	0.49	86167
RLS	$V_{cell\,min}$	0.48	0.22	5835	0.97	67289
	$V_{cell\,max}$	0.60	0.22	4599	1	50548

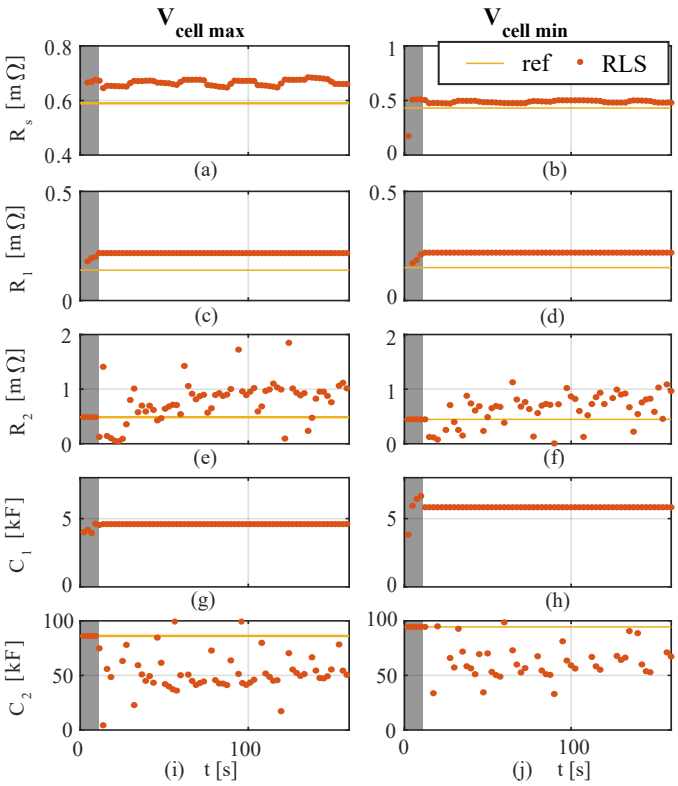

Fig. 17. Parameter estimation of the experimental results. The yellow line defines the initial value given by the VF estimation and the red one dots the estimated by the RLS filter. The gray area reflects the estimation period (t_{ch} of the first branch. From top to bottom, cell with the highest voltage: a) R_s, c) R_1. e) R_2, g) C_1, i) C_2. Cell with the lowest voltage: b) R_s, d) R_1, f) R_2, h) C_1, j) C_2.

V. CONCLUSION

This paper has exposed a comprehensive analysis to estimate the low-frequency impedance of Li-Ion battery cells via a variable-length current pulse-injection scheme delivered from the power converter. The two RC branches equivalent circuit model is taken as a reference of the impedance behavior for the frequency range tested. For the initial commissioning, the parameters are initialized through a frequency method (VF). For the real-time estimation, it is proposed a method that estimates the parameters using a RLS filter. The effects of the discretization approach and the excitation signal are analyzed in the frequency and time domain, where Bilinear approximation results in a lower error. The effects of the excitation signal are also evaluated, where the limited resolution of commercial modules reflects the higher impact on the results. For the frequency domain, the input signal requires a f_{res} capable of capturing the low frequencies of the system, and a T_{pw} large enough to avoid errors due to the limited resolution. For the RLS, the estimation is split in two stages for the different time constants, and a two-period pulse signal is proposed to energize the branch which is being estimated. The resolution is still the factor that more affects the estimation, especially for the slow branch.

Based on these previous considerations, the response of a known impedance battery has been firstly simulated to check the performance of the method. The method is validated in a

commercial battery module where the cells having the minimum and maximum cell voltages are used for the estimation. The final estimated voltage response of the LTI equivalent circuit has an error below 0.1% compared to the measured voltage.

REFERENCES

[1] M. A. Hannan, M. M. Hoque, A. Hussain, Y. Yusof, and P. J. Ker, "State-of-the-art and energy management system of lithium-ion batteries in electric vehicle applications: Issues and recommendations," *IEEE Access*, vol. 6, pp. 19 362–19 378, 2018.

[2] M. Nahvi and B. S. Hoyle, "Electrical impedance spectroscopy sensing for industrial processes," *IEEE Sensors Journal*, vol. 9, no. 12, pp. 1808–1816, Dec 2009.

[3] *ISO 12405-4:2018 Electrically propelled road vehicles –Test specification for lithium-ion traction battery packs and systems – Part 4: Performance testing*, ISO Std.

[4] A. Barai, K. Uddin, M. Dubarry, L. Somerville, A. McGordon, P. Jennings, and I. Bloom, "A comparison of methodologies for the non-invasive characterisation of commercial li-ion cells," *Progress in Energy and Combustion Science*, vol. 72, pp. 1 – 31, 2019. [Online]. Available: http://www.sciencedirect.com/science/article/pii/S0360128518300996

[5] D. Stroe, M. Swierczynski, A. Stroe, V. Knap, R. Teodorescu, and S. J. Andreasen, "Evaluation of different methods for measuring the impedance of lithium-ion batteries during ageing," in *2015 Tenth International Conference on Ecological Vehicles and Renewable Energies (EVER)*, March 2015, pp. 1–8.

[6] Z. Xia and J. A. A. Qahouq, "An online battery impedance spectrum measurement method with increased frequency resolution," in *2018 IEEE Applied Power Electronics Conference and Exposition (APEC)*, March 2018, pp. 1930–1933.

[7] C. Zhang, W. Allafi, Q. Dinh, P. Ascencio, and J. Marco, "Online estimation of battery equivalent circuit model parameters and state of charge using decoupled least squares technique," *Energy*, vol. 142, pp. 678 – 688, 2018. [Online]. Available: http://www.sciencedirect.com/science/article/pii/S0360544217317127

[8] D. Simon, *Optimal State Estimation*. Wiley-Interscience, 2006.

[9] D. Dvorak, T. Bauml, A. Holzinger, and H. Popp, "A comprehensive algorithm for estimating lithium-ion battery parameters from measurements," *IEEE Transactions on Sustainable Energy*, vol. 9, no. 2, pp. 771–779, 2018.

[10] J. Meng, D. Stroe, M. Ricco, G. Luo, and R. Teodorescu, "A simplified model-based state-of-charge estimation approach for lithium-ion battery with dynamic linear model," *IEEE Transactions on Industrial Electronics*, vol. 66, no. 10, pp. 7717–7727, 2019.

[11] M. Hossain, S. Saha, M. T. Arif, A. M. T. Oo, N. Mendis, and M. E. Haque, "A parameter extraction method for the li-ion batteries with wide-range temperature compensation," *IEEE Transactions on Industry Applications*, vol. 56, no. 5, pp. 5625–5636, 2020.

[12] S. Haykin and B. Widrow, *Least Mean Square*. John Wiley & Sons, 2003.

[13] B. Ren, C. Xie, X. Sun, Q. Zhang, and D. Yan, "Parameter identification of a lithium-ion battery based on the improved recursive least square algorithm," *IET Power Electronics*, vol. 13, no. 12, pp. 2531–2537, 2020. [Online]. Available: https://ietresearch.onlinelibrary.wiley.com/doi/abs/10.1049/iet-pel.2019.1589

[14] Q. Song, Y. Mi, and W. Lai, "A novel variable forgetting factor recursive least square algorithm to improve the anti-interference ability of battery model parameters identification," *IEEE Access*, vol. 7, pp. 61 548–61 557, 2019.

[15] B. Gustavsen and A. Semlyen, "Simulation of transmission line transients using vector fitting and modal decomposition," *IEEE Transactions on Power Delivery*, vol. 13, no. 2, pp. 605–614, April 1998.

[16] S. Grivet-Talocia and M. Bandinu, "Improving the convergence of vector fitting for equivalent circuit extraction from noisy frequency responses," *IEEE Transactions on Electromagnetic Compatibility*, vol. 48, no. 1, pp. 104–120, 2006.

[17] I. Peláez, P. García, G. Villa, and S. Saheed, "Li-ion batteries parameter estimation using converter excitation and fusion methods," in *2019 IEEE Energy Conversion Congress and Exposition (ECCE)*, 2019, pp. 2491–2498.

[18] S. B. Vilsen, S. K. Kær, and D. I. Stroe, "Log-linear model for predicting the lithium-ion battery age based on resistance extraction from dynamic aging profiles," *IEEE Transactions on Industry Applications*, vol. 56, no. 6, pp. 6937–6948, 2020.

[19] H. He, X. Zhang, R. Xiong, Y. Xu, and H. Guo, "Online model-based estimation of state-of-charge and open-circuit voltage of lithium-ion batteries in electric vehicles," *Energy*, vol. 39, no. 1, pp. 310–318, 2012, sustainable Energy and Environmental Protection 2010. [Online]. Available: https://www.sciencedirect.com/science/article/pii/S036054421200014X

[20] A. V. M. Sami Fadali, *Digital Control Engineering Analysis and Design*. Elsevier, 2013.

[21] H. He, R. Xiong, and J. Fan, "Evaluation of lithium-ion battery equivalent circuit models for state of charge estimation by an experimental approach," *Energies*, vol. 4, no. 4, pp. 582–598, 2011. [Online]. Available: http://www.mdpi.com/1996-1073/4/4/582

[22] B. Gustavsen and A. Semlyen, "Rational approximation of frequency domain responses by vector fitting," *IEEE Transactions on Power Delivery*, vol. 14, no. 3, pp. 1052–1061, July 1999.

[23] B. Gustavsen, "Improving the pole relocating properties of vector fitting," *IEEE Transactions on Power Delivery*, vol. 21, no. 3, pp. 1587–1592, July 2006.

[24] D. Deschrijver, M. Mrozowski, T. Dhaene, and D. D. Zutter, "Macromodeling of multiport systems using a fast implementation of the vector fitting method," *IEEE Microwave and Wireless Components Letters*, vol. 18, no. 6, pp. 383–385, June 2008.

[25] S. Haykin, *Adaptive Filter Theory*. Prentice-Hall, 1996.

[26] L. Ljung, *System identification: theory for the user*. Prentice Hall, 1999.

[27] S. Haykin, A. H. Sayed, J. R. Zeidler, P. Yee, and P. C. Wei, "Adaptive tracking of linear time-variant systems by extended rls algorithms," *IEEE Transactions on Signal Processing*, vol. 45, no. 5, pp. 1118–1128, 1997.

[28] Y. Zheng, M. Ouyang, L. Lu, J. Li, X. Han, and L. Xu, "On-line equalization for lithium-ion battery packs based on charging cell voltages: Part 1. equalization based on remaining charging capacity estimation," *Journal of Power Sources*, vol. 247, pp. 676–686, 2014. [Online]. Available: https://www.sciencedirect.com/science/article/pii/S037877531301522X